External surface cracked offshore pipes reinforced with composite repair system A numerical analysis

Li, Zongchen; Jiang, Xiaoli; Hopman, Hans

DOI
10.1016/j.tafmec.2021.103191

Publication date
2022

Document Version
Final published version

Published in
Theoretical and Applied Fracture Mechanics

Theoretical and Applied Fracture Mechanics 117 (2022) 103191

Contents lists available at ScienceDirect

Theoretical and Applied Fracture Mechanics

journal homepage: www.elsevier.com/locate/tafmec

External surface cracked offshore pipes reinforced with composite repair system: A numerical analysis

Zongchen Li [a,b,*], Xiaoli Jiang [a], Hans Hopman [a]

[a] Department of Maritime and Transport Technology, Delft University of Technology, 2628 CD Delft, the Netherlands
[b] Mechanical Systems Engineering, EMPA-Swiss Federal Laboratories for Materials Science and Technology, 8600 Duebendorf, Switzerland

ARTICLE INFO

Keywords:
Surface crack growth
Finite element method
Composite repair system
Stress intensity factor
FRP-to-steel interfacial bond condition

ABSTRACT

This paper conducts a numerical analysis on the external surface cracked steel pipes reinforced with Composite Repair System. A three-dimensional finite element (FE) model is developed to calculate the Stress Intensity Factor (SIF) of the surface crack, and the crack growth process is evaluated by the Paris' law. The effect of FRP-to-steel interfacial bond condition on the SIF evaluation has been considered by incorporating the cohesive zone modelling. Then the FE model is validated by the experimental results. Thereafter, major issues including "interfacial bond condition" and "reinforcement effectiveness and influential parameters" have been discussed. The results indicate the reinforcement effectiveness on reducing the SIF owes to the decreasing of stress magnitude and the crack-bridging effect. Because of the crack-bridging effect, composite reinforcement performs more efficiently on reducing the SIF at the surface point than at the deepest point of the surface crack. The negative influence of the FRP-to-steel bond condition on the surface crack growth is not as significant as on reinforcing through-thickness cracks. However, since the interfacial stiffness is sensitive to the adhesive thickness, choosing an ideal adhesive thickness to acquire a good reinforcement effectiveness and to avoid potential interfacial bond failures is recommended.

1. Introduction

Metallic pipes act as the primary way for oil and gas transportation in the offshore industry. However, they were prone to fatigue problems [1]: Under the long-term effect from dynamical loads, cracks frequently initiate from the surface of the metallic pipes and grow continually [2,3]. Repairing needs to be implemented instantly on the surface cracked metallic pipes to maintain the structural integrity. In recently decades, an advanced repairing technique—Composite Repair System (CRS)—gained its popularity in the piping industry [4], by virtue of its cost-effective, time-efficient, secondary-damage free, and easy installation [5]. In the separate study, external surface crack growth in offshore steel pipes reinforced with CRS has been experimentally investigated [6]. The study has proved the effectiveness of composite reinforcement on improving the fatigue performance of surface cracked metallic pipes. While the experimental study was restricted by the limited number of specimens, and it was infeasible for conducting sub-structural analysis.

The finite element (FE) method has been extensively applied to the investigations of composite reinforcement on cracked metallic structures over the past decades. The FE method assists users to better understand the mechanism by analysing the structural mechanical behaviour (e.g., deformation, stress concentration), fatigue indicator parameters (FIPs) such as Stress Intensity Factor (SIF) and J-integral [7–10], and bond failures [11,12]. New methods such as extended-FEM (XFEM) [13], S-version FEM [14], and the *iso*-geometric analysis (IGA) method [15,16] have been developed as efficient alternatives for handling fatigue crack growth analysis. This paper chooses the traditional FE method, which is although time consuming for both modelling and computation, it is still reliable and accurate for handling three-dimensional semi-elliptical crack analysis. Its accuracy of evaluating the FIPs has been validated, realizing the purpose of accurately predicting the crack growth process reinforced with Fibre-Reinforced Polymer (FRP). In recent years, the effect of bond failures on crack growth when employing composite reinforcement has received increasingly attention [17]. Cohesive zone modelling has been incorporated into the FE model to analyse the bond condition and its influence on the crack growth [11,12,18].

Though investigations on reinforcing through-thickness cracks,

* Corresponding author at: Mechanical Systems Engineering, EMPA-Swiss Federal Laboratories for Materials Science and Technology, 8600 Duebendorf, Switzerland.
E-mail address: zongchen.li@empa.ch (Z. Li).

https://doi.org/10.1016/j.tafmec.2021.103191
Received 16 September 2021; Received in revised form 19 November 2021; Accepted 19 November 2021
Available online 23 November 2021

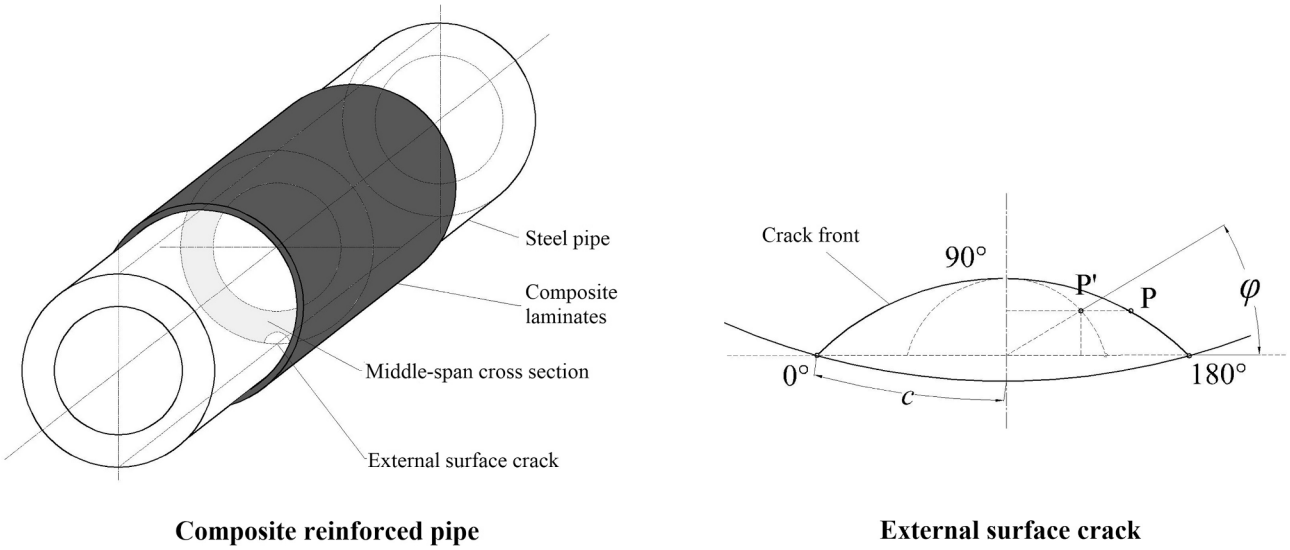

Fig. 1. The sketch diagram of the composite reinforced surface cracked pipe specimens.

Table 1
Material properties of *API 5L X65* steel.

E (Pa)	Y (Pa)	T (Pa)	v
206×10^9	4.48×10^9	5.3×10^9	0.3

Note: E is the tensile elastic modulus, Y is the yield strength, T is the tensile strength, v is the Poisson's ratio.

Table 2
Material properties of the GFRP.

E_1 (Pa)	E_2 (Pa)	E_3 (Pa)	G_{12} (Pa)	G_{13} (Pa)	G_{23} (Pa)	v_{12}	v_{13}	v_{23}
72×10^9	72×10^9	8×10^9	4.7×10^9	4.7×10^9	3.5×10^9	0.28	0.28	0.08

Note: E_i and G_{ij} are the elastic modulus and shear modulus along different directions, v_{ij} is the Poisson's ratio of the i-j plane.

Table 3
Material properties of the CFRP.

E_1 (Pa)	E_2 (Pa)	E_3 (Pa)	G_{12} (Pa)	G_{13} (Pa)	G_{23} (Pa)	v_{12}	v_{13}	v_{23}
230×10^9	25×10^9	25×10^9	5.5×10^9	5.5×10^9	3.9×10^9	0.33	0.33	0.054

researchers believed the crack-induced debonding would occur at the FRP-to-steel interface, which decreased the effectiveness on reducing the crack growth rate [11]. However, through the previous studies [19], we found these conclusions might not be directly applied when reinforcing surface cracks: the debonding induced by surface crack might not be as serious as that induced by through-thickness cracks, and its effect might be less significant on surface crack growth. However, the potential of the interfacial failure or stiffness degradation should be considered to achieve accurate evaluation of the crack growth rate and residual fatigue life. Thus, further analysis on the interfacial bond condition and its effect on surface crack growth is necessary. In addition, the investigations of composite reinforcement on surface cracked steel plates [10,19] and on surface cracked pipes [6] indicated some diverse conclusions in terms of reinforcement schemes and key influential parameters. Therefore, an in-depth FE analysis on external surface crack growth in steel pipes reinforced with composite is essential.

Given those concerns, this paper conduct a FE analysis to investigate the effect of composite reinforcement on the external surface crack growth in metallic pipes. Section 2 develops a three-dimensional FE model to evaluate the Stress Intensity Factor (SIF) of the surface crack, followed by the experimental validation in Section 3. Section 4 analyses and discusses two major issues from the "interfacial bond condition" and the "reinforcement effectiveness and influential parameters" perspectives. Finally, Section 5 draws the main conclusions.

2. Finite element modelling

In this section, the FE models of surface cracked metallic pipes reinforced with CRS are built. Within the FE model, FRP-to-steel interfacial bond condition is analysed by means of the cohesive zone modelling, and its effect on the SIFs along the crack front is taken into consideration.

2.1. Material properties and the interfacial properties

The sketch diagram of the FE model is shown in Fig. 1, indicating a semi-elliptical surface crack embedded on the external surface of a steel pipe, located at the mid-span cross-section. Point A and B represent the deepest point and the surface point of the surface crack, respectively. The "a" is the crack depth, and "$2c$" is the crack length. The eccentric angle "β" ranging from 0° to 180° identifies the location of point "P" on the crack front. Composite laminates are wrapping around the pipe. Four materials are employed, which are steel, Glass-FRP (GFRP), Carbon-FRP (CFRP), and adhesive. The pipe substrate adopts the stainless steel *API 5L X65* conforming to API SPEC 5L code [20] for subsea scenarios. One layer of GFRP laminate, which uses the E-glass fibre weave fabric, is adopted as the contact inhibitor between the steel substrate and CFRP laminates, concerning the CFRP-to-steel galvanic corrosion. The CFRP laminate applies the Toray T700S series unidirectional fabric, and the adhesive layer adopts the Faserverbundwerkstoffe® L20 resin epoxy with hardener EPH 161 [21]. The detailed material properties are listed in Tables 1 to 4. Note that each corresponding supplier provides the material properties.

In addition to the material properties of the adhesive layer, we incorporate a cohesive zone model to simulate the interfacial bond condition, using the mixed-mode bi-linear traction-separation law, as indicated in Fig. 2.

For the Mode-I case, the separation displacement δ_n^0 when the trac-

Table 4
Material properties of the adhesive layer and the properties of the mixed-mode traction-separation model.

	E (Pa)	T (Pa)	G (Pa)	f_t (MPa)	δ_n^0 (mm)	δ_n^f (mm)	K (MPa/mm)	G_c (N/mm)	ε_f
Mode-I (tension)	3.4×10^9	70.2×10^6	1.019×10^9	70.20	0.004	0.019	17,000	0.667	0.095
Mode-II (shear, tangential)				56.16	0.011	0.16	5095	4.488	

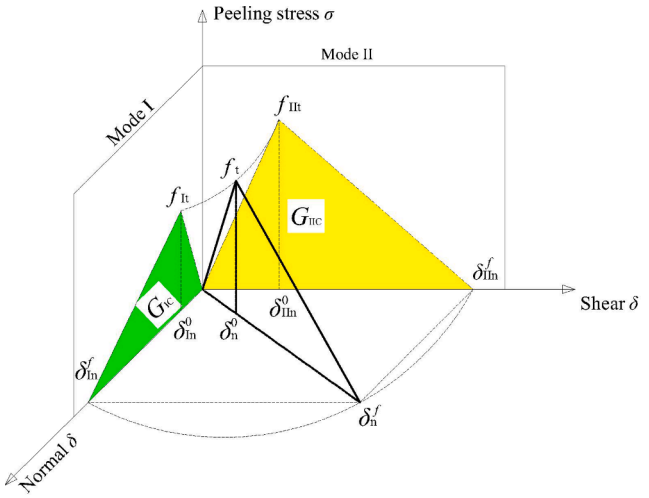

Fig. 2. The mixed-mode traction-separation law.

tion stress reaches the maximum f_{It}, is

$$\delta_{\mathrm{In}}^0 = \frac{t_a \bullet f_{\mathrm{It}}}{E} \tag{1}$$

where t_a is the thickness of the adhesive.

The energy release rate is the triangle area surrounded by the curve and the coordinate axis, which is

$$G_{\mathrm{IC}} = \frac{1}{2} f_{\mathrm{It}} \bullet \delta_{\mathrm{In}}^f \tag{2}$$

where δ_{In}^f is the separation displacement when debonding/delamination occurs, which is

$$\delta_{\mathrm{In}}^f = \varepsilon_f \bullet \mathrm{t_a} \tag{3}$$

where ε_f is the elongation ratio.

The slope of the ascending part equals to the shear stiffness of the adhesive layer, which is

$$k = \frac{f_{\mathrm{It}}}{\delta_{\mathrm{In}}^0}. \tag{4}$$

For the Mode-II case, the variables of the traction-separation law is calculated using the method given by Ref. [22]. G_{IIC} is calculated as

$$G_{\mathrm{IICs}} = G_{\mathrm{IICt}} = 31 \bullet \left(\frac{\mathrm{f_{IIt}}}{\mathrm{G}}\right)^{0.56} \bullet \mathrm{t_a}^{0.27}. \tag{5}$$

where G is the shear modulus of the adhesive. The traction force is estimated as

$$f_{\mathrm{IIt}} = 0.8 \bullet \mathrm{T}, \tag{6}$$

and δ_{IIn}^0 is calculated as

$$\delta_{\mathrm{IIn}}^0 = \frac{t_a \bullet f_{\mathrm{IIt}}}{G}, \tag{7}$$

δ_{IIn}^f is calculated as

$$\delta_{\mathrm{IIn}}^f = \frac{2G_{\mathrm{IIC}}}{f_{\mathrm{IIt}}}, \tag{8}$$

The interfacial properties calculated by Eqs. (1)–(8) are listed in Table 4. The degree of the interfacial stiffness degradation is represented by the scalar stiffness degradation variable (SDEG) from 0 to 1. Fully debonding occurs when meeting the condition indicated in Eq. (9), where the SDEG value evaluated by the FE model exceeds 1.0.

$$\left(\frac{G_{\mathrm{I}}}{G_{\mathrm{IC}}}\right)^2 + \left(\frac{G_{\mathrm{IIs}}}{G_{\mathrm{IICs}}}\right)^2 + \left(\frac{G_{\mathrm{IIt}}}{G_{\mathrm{IICt}}}\right)^2 = 1, \tag{9}$$

where G_{IICs} and G_{IICt} stand for the Mode-II energy release rate in two shear directions.

2.2. Modelling strategy

The FE modelling and analysis are conducted in ABAQUS® 2021 [23]. The reason of choosing the ABAQUS package is that it is capable of evaluating the interfacial stiffness degradation by implementing the cohesive zone modelling. Fig. 3 illustrates the three-dimensional model and its meshing condition. The size of the model conforms to the test specimens in the previous experimental study. The length, external diameter and thickness of the steel pipe are 2,000 mm, 168.3 mm, and 12.7 mm, respectively. Each composite laminate is 0.35 mm thick, while the adhesive layer is 0.2 mm thick. A quarter surface crack as a semi-elliptical shape is modelled at the mid-bottom of the pipe, locating at the X-Y plane, as shown in the Fig. 3b. A bending moment of 6.0385×10^7 kN•m is applied on the pipe, which is identical to the experimental bending moment generated by the four-point bending set-up. This bending moment generates 60% of the yield strength, i.e., 268.8 MPa, around the cracked area. The SIF along the crack front is calculated via the contour integral method, which is capable to accurately evaluate the SIF along a crack front. Please note the SIF is evaluated through linear facture mechanics, therefore the plastic zone effect around the cracked area is excluded in this paper.

The steel pipe, the five layers of composite laminates, and the adhesive layer between the steel substrate and the GFRP layer composite the FE model together. The FE model is developed based on the physical situation that the overall patch thickness (including adhesive layer and the composite laminates) is 1.95 mm. Since the experimental study indicated no delamination failures within the FRP laminates occurred, we modelled all composite laminates as a whole. The different layers of composite laminates were merged together while remaining their own material properties and fibre directions. While each laminate remains its own material properties and orientation. One layer of adhesive is modelled between the CFRP laminates and the steel substrate through the cohesive zone modelling. The steel pipe excludes the crack front region, and the composite laminates, apply the 20-node quadratic brick element C3D20, while the crack front area adopts the 15-node quadratic triangular prism element C3D15. The reason of adopting quadratic brick element, including the C3D20 and C3D15 element is they are excellent for three-dimensional linear elastic calculations. The C3D15 element is applied to meet the requirement of the wedge element shape at the crack front when using contour integral method. The standardized 8-node three-dimensional cohesive element COH3D8 is used in the adhesive layer, to simulate the interfacial bond condition between the steel substrate and the composite laminate. Different meshing methods are adopted to ensure a robust and accurate evaluation. The FE model

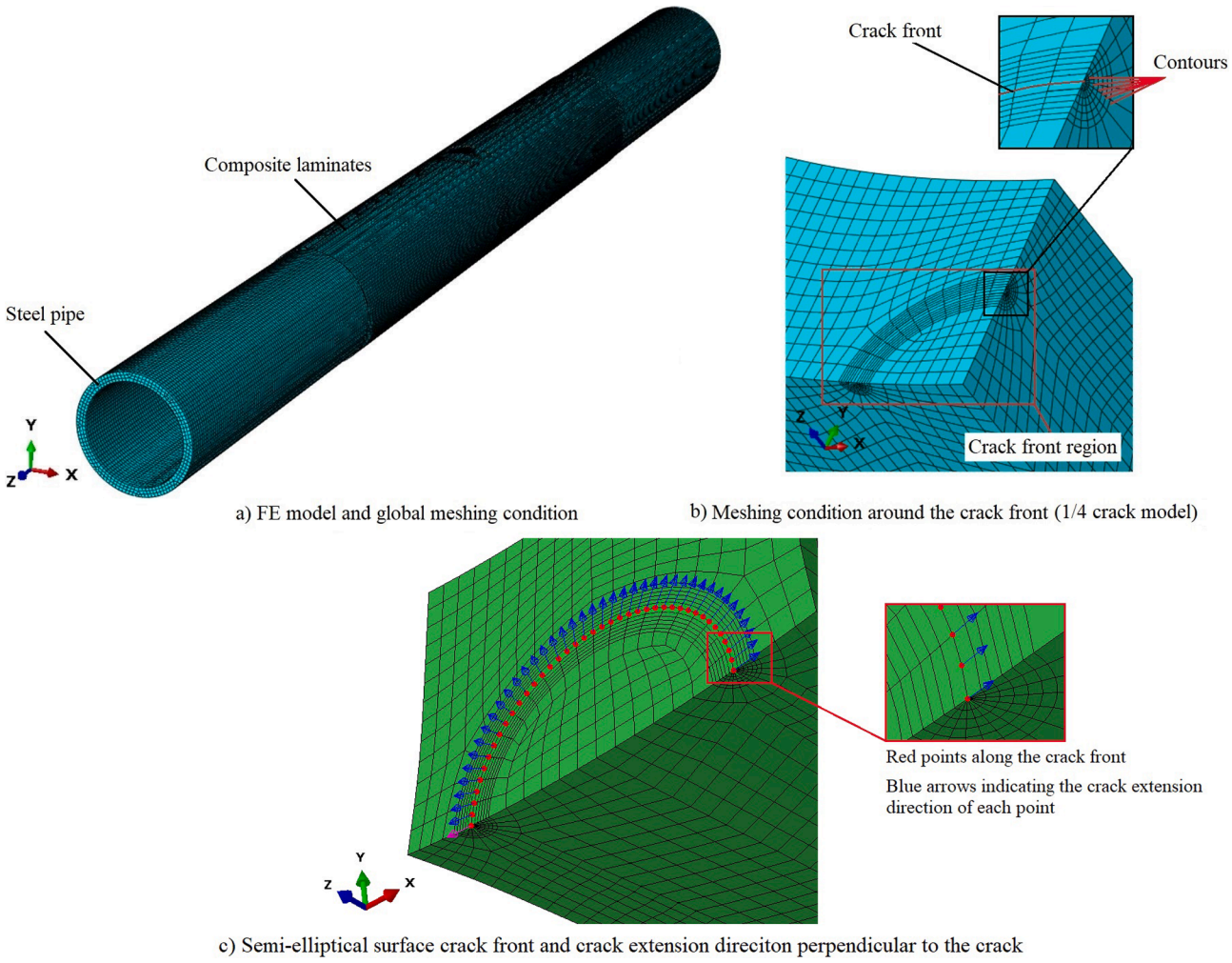

Fig. 3. The FE model and the meshing condition: (a) the whole model and global meshing; (b) model and meshing around the crack; (c) Crack front and the set-up of crack extension direction.

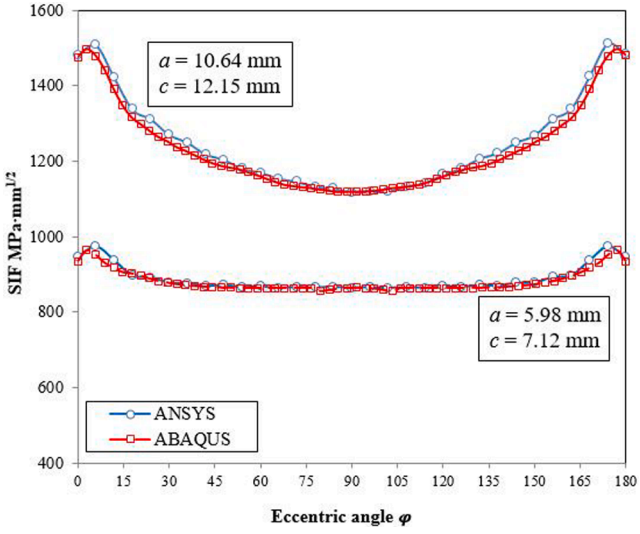

Fig. 4. The comparison of SIF evaluation by using ABAQUS and ANSYS for a small crack and a large crack in steel pipes.

excluded the crack front region and the adhesive layer adopt the hexahedron element by the structural meshing method. While the crack front region and the adhesive layer applies the sweep meshing methods, using wedge element and hexahedron element, respectively. Under the premise of accurate evaluation, different element sizes are assigned in different areas of the FE model to reduce the computational time. The size of the wedged elements in the crack front region is controlled by the six concentric contours and 24 divisions on each of those, as indicated in Fig. 3b. The diameter of the external contour is 1.0 mm, and the crack front has been divided into 22 pieces. The mesh size of the area in the steel pipe adjacent to the crack front area, as well as the adhesive layer and the composite laminates are set as 1.0 mm, while the size of the pipe away from the crack front area is set as 5.0 mm.

2.3. SIF evaluation and verification

This SIF evaluation using the contour integral method in ANSYS has been verified in the previous study [2]. In this paper, since ABAQUS package is chosen for FE modelling, the accuracy of evaluating SIF of surface cracks needs to be verified by comparing the SIF results with the results simulated by ANSYS Workbench 2021 [24]. Fig. 4 shows the comparison of the SIF results of a small crack (a = 5.98 mm, c = 7.12 mm) and a large crack (a = 10.64 mm, c = 12.15 mm) using two FEM

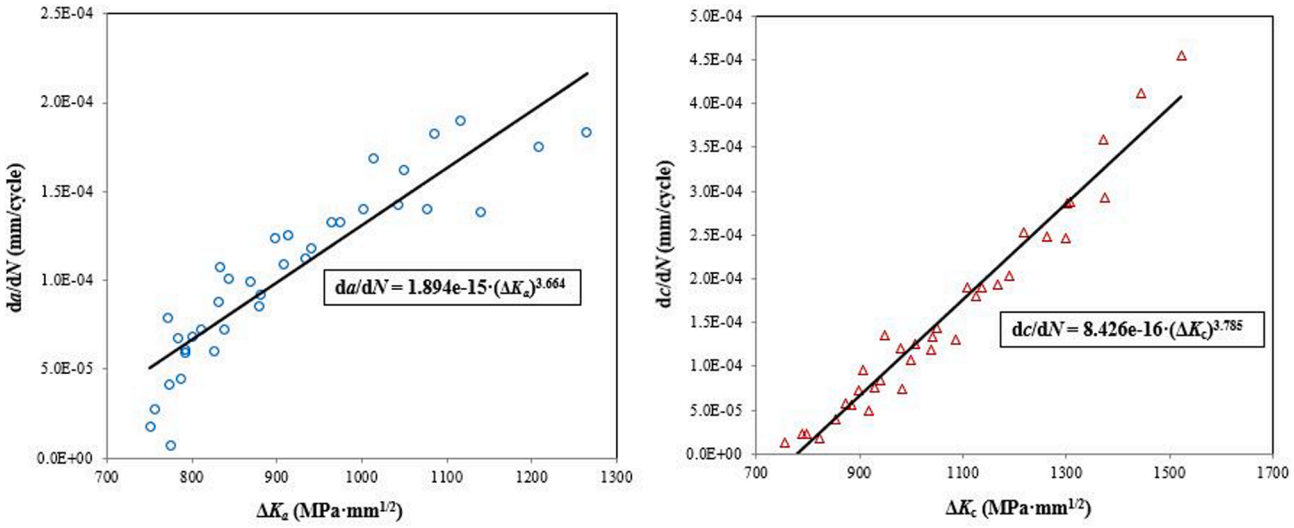

Fig. 5. Evaluation of the Paris' constants (C and m) from da/dN versus ΔK_{Ia}, and dc/dN versus.ΔK_{Ic}

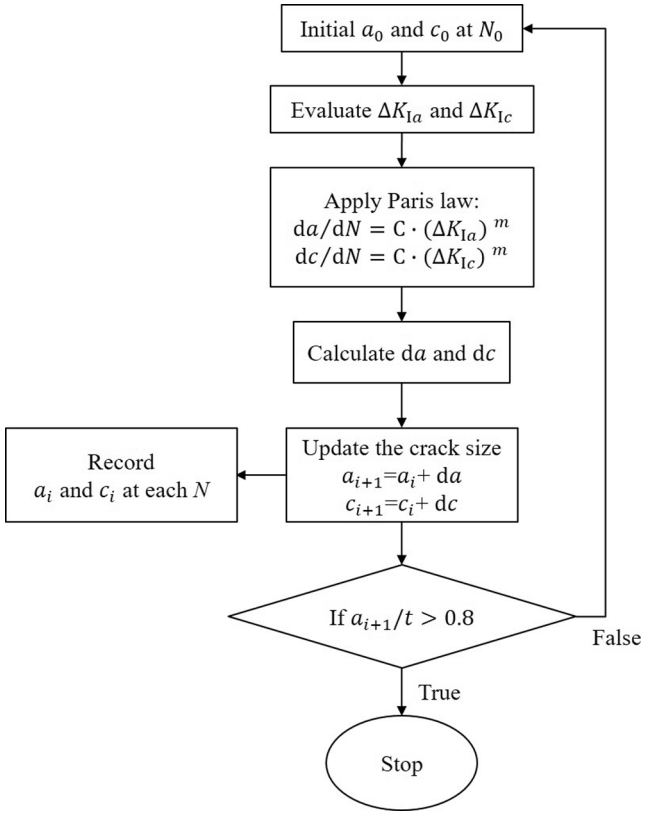

Fig. 6. The program of evaluating surface crack growth.

packages. The comparison illustrates the ABAQUS package is able to evaluate the SIF along the crack fronts accurately, with a maximum error of less than 1%. The detailed SIF results along the crack front of the two cracks evaluated by ABAQUS and ANSYS are listed in Table A1 &A2 in Appendix A, respectively. This is to be expected because the simulation in both packages applied the contour integral method with the same contour numbers and contour sizes. Technologies, the model simulated in ABAQUS package should provide slightly more accurate results on account of the more regular shaped elements within the areas adjacent to the contours—the hexahedral elements, rather than using the tetrahedral elements within the ANSYS Workbench package. Table A2.

Table 5
The configurations of the FE models for experimental validation.

Name	Initial crack size (mm)		CFRP wrapping scheme	Bond length (mm)
	Crack depth a	Half-crack length c		
PE-1 FE	4.29	5.80	/	/
PE-1-R FE	5.98	7.12	L-L-L-H	1,000
PE-2 FE	5.34	6.53	/	/
PE-2-R FE	5.24	6.13	L-L-L-H	1,000
PE-3 FE	5.34	5.78	/	/
PE-3-R FE	5.92	6.235	L-L-L-H	1,000
PE-1-R600 FE	6.10	7.465	L-L-L-H	600
PE-1-R8 FE	5.92	7.28	L-L-L-H-L-L-L-H	1,000
PE-1-R45 FE	4.99	6.525	Inversely diagonal	1,000

3. Experimental validation

Since offshore structures are reaching their original design life, effective fracture mechanics computational models are required, in order to ensure continued safe operations. In this section, thus the Paris' law was combined with numerical technique previously discussed to analyse surface crack growth in pipes subjected to bending. First, the Paris' constants of the steel are evaluated based on the experimental results of the un-reinforced steel pipe specimens. Then, the surface crack growth in composite reinforced models is evaluated by incorporating the SIF into the Paris' law [25]. Hence, the FE model can be validated by comparing the evaluated crack growth results with the experimental data.

The SIFs without composite reinforcement are calculated through the validated FE model, then the surface crack growth rate along the depth or length directions are evaluated through

$$da/dN = C \cdot (\Delta K_{Ia})^m \quad (10)$$

$$dc/dN = C \cdot (\Delta K_{Ic})^m \quad (11)$$

where da/dN and dc/dN are the crack growth rate along the depth or length direction. C and m are the Paris' constants. Fig. 5 shows the determined C and m based on the experimental results.

Fig. 5 clearly shows that the values of C and m for surface crack growth along the depth direction and the length direction are different. Hence the constants for the depth and length direction are $C_a = 1.894 \times$

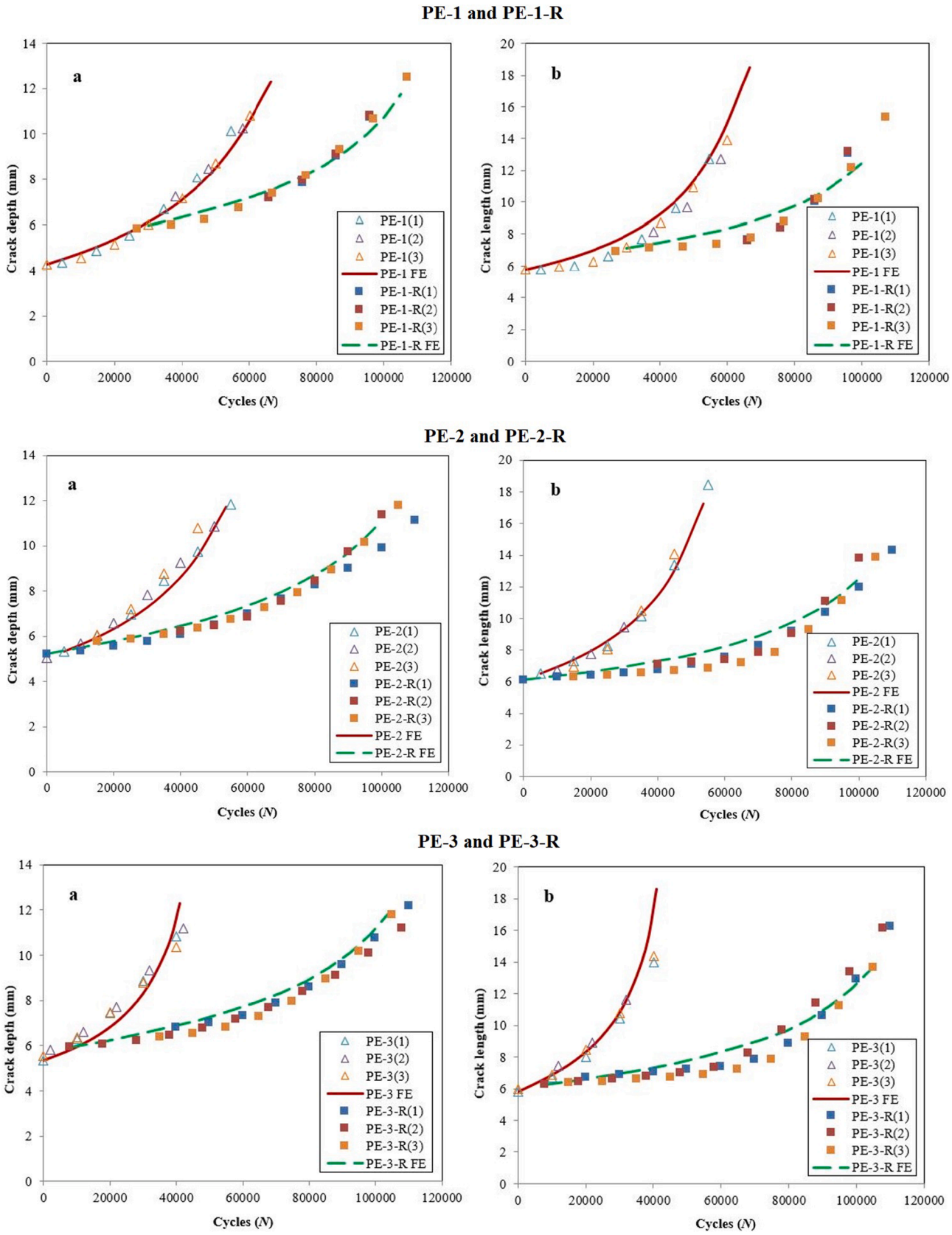

Fig. 7. The comparison of theoretical results and experimental results using the default-reinforcement scheme: a) along depth direction; b) along length direction.

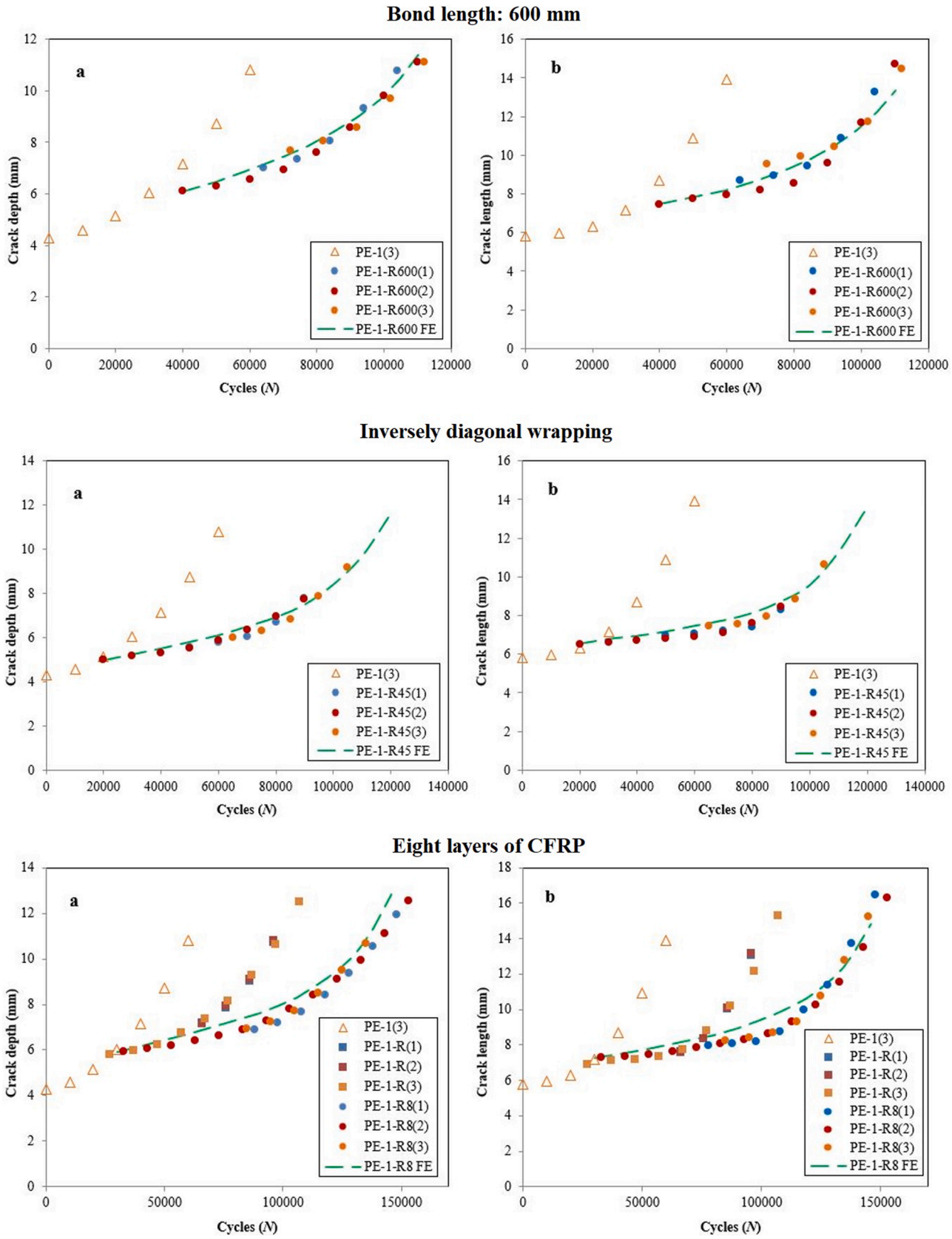

Fig. 8. The comparison of theoretical results and experimental results using different reinforcement schemes, namely 600 mm bond length (PE-1-R600), inversely diagonal wrapping pattern (PE-1-R45), and applying eight layers of CFRP (PE-1-R8).

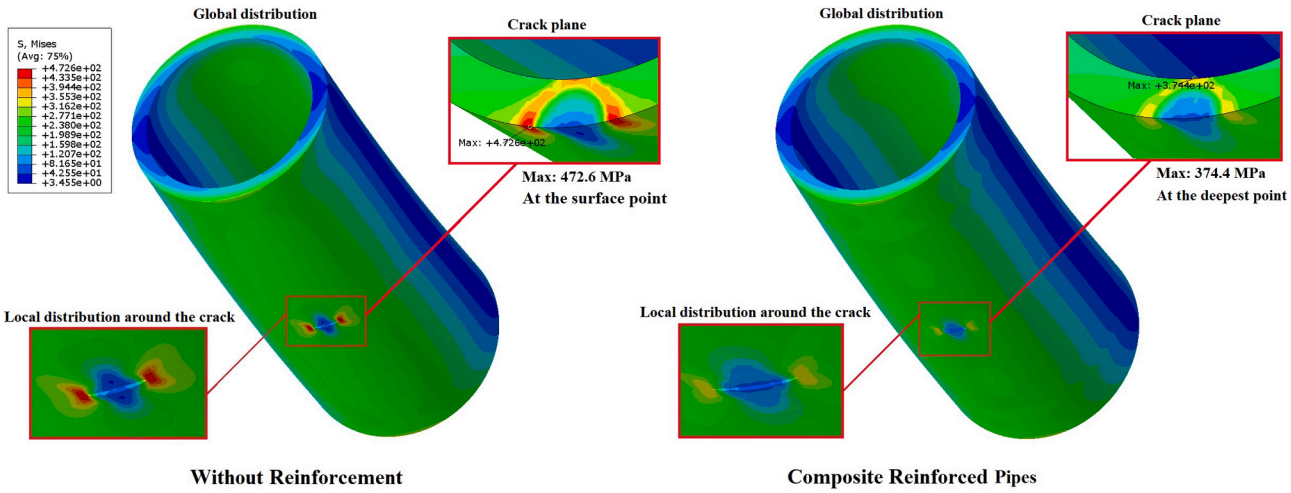

Fig. 9. Global and local von Mises stress distribution of the pipe model with large surface crack (a = 10.64 mm and c = 12.15 mm) under the bending moment of.6.0385 × 10^7kN•m

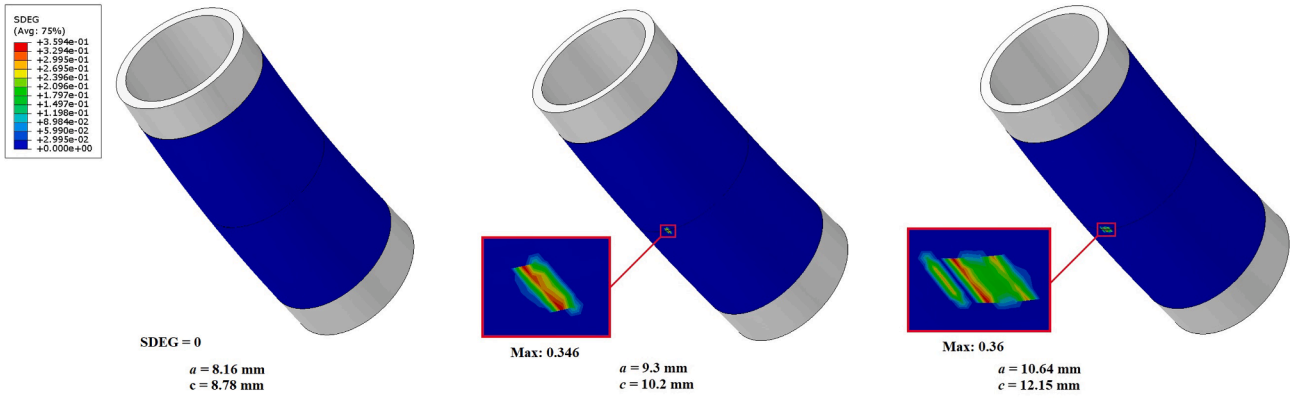

Fig. 10. Interfacial stiffness degradation with different crack sizes along with the crack growth process under the bending moment of.6.0385 × 10^7kN•m

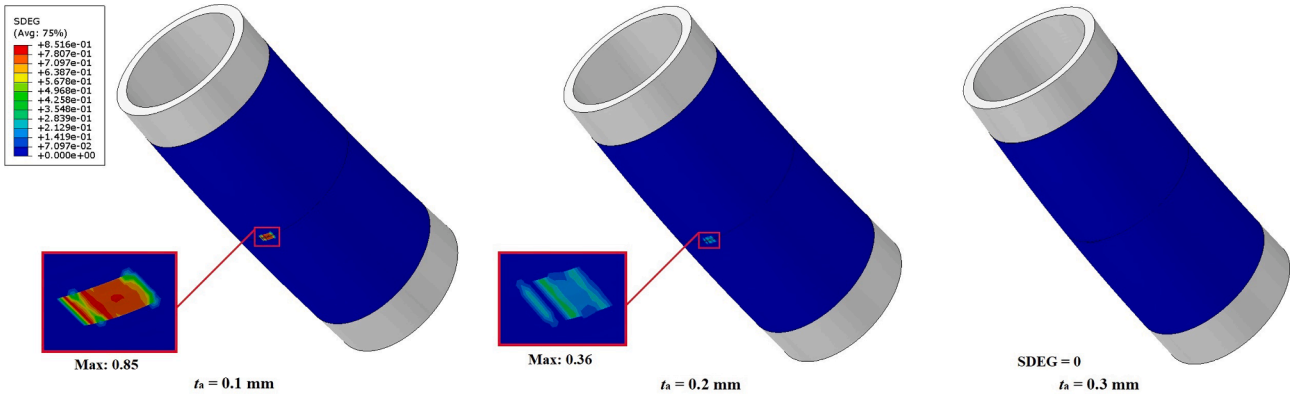

Fig. 11. Interfacial stiffness degradation with different adhesive thickness, under the bending moment of.6.0385 × 10^7kN•m

10^{-15} and $C_c = 8.462 \times 10^{-16}$, respectively, and $m_a = 3.664$ and $m_c = 3.785$ respectively. Note that the unit for SIF is MPa•$mm^{1/2}$, and the unit for da/dN is mm/cycle. After that, surface crack growth of the composite reinforced FE models along the depth or the length direction is evaluated through the process indicated by the flow chart in Fig. 6.

FE models corresponding to the test specimens from the previous experimental study [6] (e.g., initial crack size, layers of laminates and orientation) are built for the purpose of experimental validation. The modelling process follows the strategy as described in Sub-section 2.2. The initial crack size of the FE models adopts the data of one test specimen from each group. The initial crack size of each FE model and reinforcing method is listed in Table 5. Take PE-1-R FE as an example, the name follows the same rule of the test specimen while adding the FE as the indication of a FE model, where “PE” represents “pipe external crack”, “1″ means the first category of the crack size out of three different sizes in total, and ”R“ means with composite reinforcement. The ending without an ”R“ means the model is without reinforcement, regarded as a control model. The number behind ”R“ indicates different

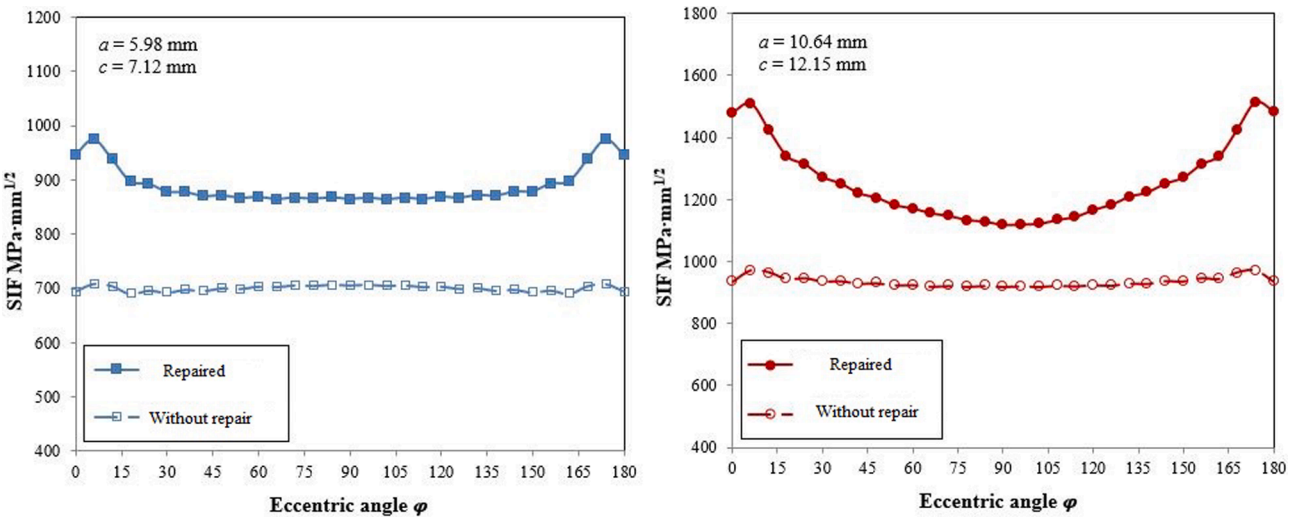

Fig. 12. The SIF distributions along the crack front of a small crack (left) and a large crack (right), under the bending moment of.6.0385 × 10^7kN•m

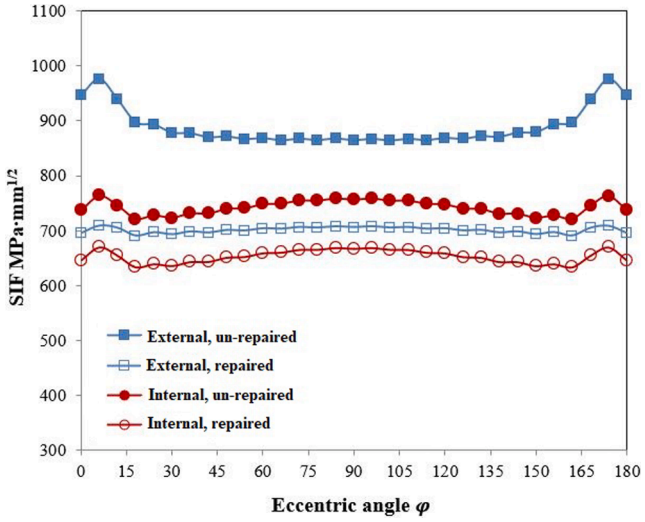

Fig. 13. The comparison of the SIF results between the external surface crack and the internal surface crack reinforced by composite.

Table 6
Specimen configuration of steel pipes with different aspect ratios.

Model No.	*a* (mm)	*c* (mm)	*a/c*	SIF reduction at the deepest point	SIF reduction at the surface point
1	3.0	12.0	0.25	21.9%	20.8%
2	3.0	6.0	0.5	18.4%	23.2%
3	4.5	6.0	0.75	17.8%	26.4%
4	6.0	6.0	1.0	16.9%	27.8%
5	6.0	4.5	1.25	14.8%	22.9%
6	6.0	3.0	2.0	12.3%	20.8%

reinforcement strategy, say ”600 mm“ bond length comparing to the default 1,000 mm, ”8″ for eight layers of CFRP laminates comparing to the default four layers, and “45″ stands for the inversely diagonal wrapping pattern (45°/135°/45°/135°) comparing to the default L-H-L-H wrapping pattern (0°/90°/0°/90°). Note that although the initial crack sizes of the reinforced model (e.g., PE-1-R FE) and its control model (PE-1 FE) are different, they were initiated from notches with the same size from the experimental specimens. Please refer to Ref. [6] for detailed information.

Table 7
Configurations of steel pipe models with different dimensions, and the results of the SIF decrease.

Model No.	*D* (mm)	*t* (mm)	*D/t*	SIF reduction at the deepest point	SIF reduction at the surface point
1	168.3	10.97	15.34	20.1%	29.5%
2	168.3	12.70	13.25	18.4%	27.3%
3	168.3	14.27	11.79	17.3%	26.0%
4	168.3	18.26	9.22	15.3%	23.8%
5	168.3	21.95	7.67	14.1%	22.6%
6	219.1	12.70	17.25	17.5%	28.2%
7	273.0	12.70	21.50	16.4%	25.3%
8	323.8	12.70	25.40	14.7%	24.6%

The SIF of surface cracks in each model, specifically K_{Ia} at the deepest point and K_{Ic} at the surface point are evaluated by the FE analysis. The SIF results at the deepest point and at the surface point of PE-1 and PE-1-R model with different crack sizes during the crack propagation process are listed in Table B1 in Appendix B, as an example. Then the program indicated in Fig. 6 using the Paris' law, predicts crack growth along the depth direction and the length direction. The crack increment Δa and Δc is calculated by the integral calculation of Eqs. (10) and (11), assigning a range of cyclic intervals ΔN. Eventually, the surface crack size, namely the crack depth a and the half crack length c, corresponding to their cyclic counts are obtained. The results can then be compared with the experimental results for validation purpose. Please note the balance between the computational accuracy and the time consuming is important.

Figs. 7 and 8 shows the comparison between the theoretical results and the experimental results of surface crack growth. The figures indicate that the theoretical evaluations match well with the experimental results when using composite to repair the cracked surface of the steel pipes, which means that the FE model combined with the Paris' law can accurately predict the residual fatigue life of surface cracked steel pipes reinforced with composite. In addition, the results indicate that FRP reinforcement has significantly decreased the surface crack growth and prolonged the residual fatigue life of cracked models. For instance, without reinforcement, the PE-1(3) specimen only has a residual fatigue life of around 30,000 cycles start from the crack depth $a = 6.02$ mm to the crack depth $a = 10.8$ mm. While using eight layers of CFRP laminates to reinforce the surface cracked pipe at the same statue ($a = 6.02$ mm)

has prolonged the residual fatigue life to 135,000[1].

4. Results and discussions

In this section, the theoretical results are presented and discussed from two main aspects: the interfacial bond condition and the reinforcement effectiveness. Analysing the interfacial bond condition is necessary since it acts as an important factor of influencing the effectiveness of the reinforcement. The SIF, as a fatigue indicator parameter, determines the effectiveness of the FRP reinforcement, helping us to understand the mechanism of the FRP reinforcement on external surface cracks. Please note all results in Sub-section 4.1, 4.2 & 4.3 exclude Sub-section 4.3.4 are calculated based on the pipe diameter of external diameter $R = 168.3$ mm and pipe wall thickness $t = 12.7$ mm, consistent to the FE model in Section 3. A bending moment of $M = 6.0385 \times 10^7$ kN•m is applied on all models in this section.

4.1. Stress distribution around the surface crack

The von Mises stress distributed globally throughout the pipe model and locally around the surface crack is shown in Fig. 9. The SIF results along the crack front is shown in Fig. 12. The stress distribution results indicate the composite reinforcement with four layers of CFRP laminates has significantly decreased the stress concentration, the maximum stress value drops from 472.6 MPa to 374.6 MPa, by 20.7%. Moreover, the position that has the maximum stress value has shifted from the surface point to the deepest point along the crack front because of the composite reinforcement. The stress value at the surface point drops from 472.6 MPa to 353.4 MPa, by 25.2%, while the stress value at the deepest point only drops 9.0%, from 411.3 MPa to 374.4 MPa. This phenomenon is an evidence that the composite reinforcement performs better on decreasing the crack growth along the length direction than along the depth direction.

4.2. Interfacial bond condition

4.2.1. Interfacial bond condition along with the surface crack growth

The interfacial bond condition along with the surface crack growth is analysed. Crack sizes were extracted from the experimental specimen of PE-1-R(3) from the beginning of the crack growth to a larger crack size before penetrating the pipe wall. Each adjacent crack size has an interval of 10,000 cycles. The FE model in this part is in accordance with the FE models in Section 2 using the default repairing method. The interfacial bond conditions of models with different crack sizes, represented by the SDEG value, are shown in Fig. 10. It was only until the crack grew to a relatively large size ($a = 9.3$ mm, $c = 10.2$ mm) did the interfacial stiffness began to decrease, showing the maximum SDEG value reached 0.346. Then the maximum SDEG value slightly grew to 0.36 when the crack grew to the largest size, and the area of stiffness degradation expanded with a relatively low value. The SDEG value, which is smaller than 1.0, indicating no debonding have happened during the crack growth process. Therefore, since the interface stiffness degradation did not occur until the very late stage of the crack growth process, and the value of the SDEG is relatively low, its negative influence on decreasing the crack growth rate should be insignificant.

4.2.2. Adhesive thickness

The interfacial bond condition with different adhesive thickness is analysed as well, as shown in Fig. 11. In this part, a large crack size of $a = 10.64$ mm and $c = 12.15$ mm is selected for the model. Three different adhesive layer thickness, namely 0.1 mm, 0.2 mm and 0.3 mm are built, using the default repairing method as described in Section 2. The interfacial bond properties for each adhesive thickness is calculated by the Eqs. (1)–(8). The results indicate thinner adhesive layer brings more risks to the failure of the interfacial bond, resulting in the maximum SDEG value of 0.85. While interfacial stiffness did not happen on the model with 0.3 mm adhesive thickness.

From previous studies, we learned that a relatively thin thickness of the adhesive could promote the effectiveness of FRP reinforcement. However, considering the interfacial stiffness degradation might cause potential failures, choosing an ideal adhesive thickness to acquire a good reinforcement effectiveness and to avoid the interfacial failure is recommended.

4.3. Reinforcement effectiveness and influential parameters

In this sub-section, the FRP reinforcement effectiveness on different crack sizes, and comparison between external surface cracks and internal surface cracks are analysed. Besides, influential parameters in terms of crack aspect ratio, dimensions of the pipe are discussed. However, influential parameters such as layers of bond, bond length, and orientation of the laminates are excluded in this paper, since they have been discussed through the previous experimental study [6] and share similar conclusions with the investigations on reinforcing internal surface cracked pipes [9].

4.3.1. Crack sizes

Two crack sizes are applied for the analysis, namely a small one ($a = 5.98$ mm, $c = 7.12$ mm) and a large one ($a = 10.64$ mm, $c = 12.15$ mm). They are both obtained from the experimental results of specimen PE-1-R(3), as shown in Fig. 6, corresponding to the cyclic number of around 30,000 and 100,000, respectively. The purpose of analysing SIFs of two crack sizes is to better understand the mechanism of FRP reinforcement on reduction of the surface crack at different crack growth stages.

Fig. 12 shows the SIF results of both un-repaired crack and repaired crack using the default reinforcement method. It indicates the diverse effect of composite reinforcement on different crack sizes: composite reinforcement decreases the SIFs at the deepest point and the surface point of 18.37% and 27.32% respectively for a small crack, while decreases 17.74% and 35.68% respectively for a large crack. The results of SIF reduction indicate that along with the crack growth, FRP reinforcement performs slight less efficient on decreasing the crack growth along the depth direction, while vice versa along the length direction. This might owe to the fact the distance between the deepest point and the FRP laminates becomes larger when a crack grows bigger, while the "crack-bridging effect" might offer more bond effect on the surface point with a relatively larger crack.

4.3.2. Comparison between external surface cracks and internal surface cracks

In a previous study of FRP reinforcement on internal surface cracked pipes [9], it was concluded the reinforcement has equal effectiveness on the SIFs of the deepest point and the surface point. However, it might not be the case for reinforcing external surface crack pipes, due to the fact the FRP laminate has a direct contact with the surface crack. Owing to the crack-bridging effect, composite reinforcement may performs more efficient on decreasing crack growth along the length direction than along the depth direction. In this part, both un-reinforced and reinforced internal surface cracked pipe models are built, using the same crack size

[1] Please note the fatigue phenomenon of fatigue life prolongation is analysed by the same methodology as described in the flow chat in Fig. 6, combing the SIF evaluation with the Paris' law. The initial crack sizes were obtained from the test specimens, such as $a = 5.98$ mm and $c = 7.12$ mm from PE-1(3). Then, both of the un-reinforced crack and the reinforced crack were modelled based on the same initial crack size from the un-reinforced test specimen. Thereafter, these two FE models ran independently and evaluated the crack propagation curves (crack size versus cyclic index) until they reached the same crack depth (e.g., 80% of the pipe wall thickness). Via such methods, their residual fatigue life (the cyclic numbers from beginning to the end) can be obtained and compared.

($a = 5.98$ mm, $c = 7.12$ mm) as the external surface cracked pipe models.

Fig. 13 shows the comparison results of the composite reinforcement on both external and internal surface cracked pipe models. FRP reinforcement decrease the SIFs along the internal surface crack front of around 12%. While the reinforcement performs more efficient on the surface point than on the deepest point of the external surface crack, of 27.3% and 18.4% respectively. Therefore, the results prove the additional effect of the crack-bridging effect on decreasing the SIF at the surface point. The results can speculate that composite reinforcement decrease the SIF of the external surface crack not only through decreasing the stress value around the crack, but also through the crack-bridging effect.

4.3.3. SIF reduction on cracks with different crack aspect ratios

SIFs of surface cracks with six aspect ratios ranging from 0.25 to 2.0 are analysed. The detailed crack sizes of each FE model, as well as the SIF reduction results of the deepest point and the surface point are shown in Table 6. It illustrates that the SIF reduction of the deepest point is decreasing that with the increasing of the crack aspect ratio. While there is no clear trend of the SIF response along the surface point. In light of the models from No. 2 to No. 4, which have the same crack length, the SIF reduction proportion increases with the increasing of the surface depth. For models of No. 4 to No. 6 with the same crack depth, the SIF reduction proportion also shows a positive correlation with the crack length. Since the crack growth along the depth direction has a special significance in terms of preventing the pipe leakage, the composite reinforcement is more efficient on surface cracks with smaller aspect ratio.

4.3.4. SIF reduction on cracks in steel pipes with different dimensions

API 5L series pipes for the offshore transporting usage with eight different dimensions indicated by the D/t ratios [20] are analysed. The configurations of the reinforced pipes with different external diameter and wall thickness are listed in Table 7. Four different external diameter ranging from 168.3 mm to 323.8 mm with five different wall thickness from 10.97 mm to 21.95 mm are studied: five incremental pipe wall thickness has been discussed with $D = 168.3$ mm, while four incremental external diameter has been analysed with $t = 12.7$ mm. These dimensions are chosen owing to their frequently usage in the offshore piping industry.

Table 7 illustrates that the reinforcement effectiveness decreases with the increasing of wall thickness under the same external diameter of 168.3 mm. In light of the models of $t = 12.7$ mm, i.e., Model No. 2, and No. 6 to No.8, the effectiveness decreases with the increasing of external diameter. Hence, the composite reinforcement is less effective on pipes with larger external diameter and thicker wall. In cases of reinforcing pipes with large dimensions, it is recommended to employ more layers of CFRP with high elastic modulus for achieving a satisfying decrease of crack growth rate.

5. Conclusions

This paper conducts a numerical investigation on external surface crack growth in steel pipes reinforced with composite repair system subjected to bending. The developed three-dimensional FE model, which considered the FRP-to-steel interfacial bond condition, is able to evaluate the SIF of the surface crack rationally. Thereafter, based on the validated FE model, the numerical results from the "interfacial bond condition" and the "reinforcement effectiveness and influential parameters" perspectives have been analysed and discussed. Hereby are the major conclusions.

- The FE method is able to accurately evaluate the SIF of the external surface crack in the composite reinforced steel pipes subjected to bending.
- The analysis of the composite reinforcement on reducing the SIF indicates the reinforcement effectiveness owes to the decreasing the stress value and the crack-bridging effect. The analysis on the SIF further proves that composite reinforcement performs more efficiently on reducing the SIF at the surface point than at the deepest point, owing to the crack-bridging effect.
- The analysis on the FRP-to-steel interfacial bond condition indicates the interfacial stiffness degradation only happened at a later stage of the cracking process, and the value of the SDEG is relatively low. Therefore, its negative influence on decreasing the crack growth rate should be insignificant.
- The interfacial stiffness degradation is sensitive to the adhesive thickness and crack sizes. In reality, we recommend to analyse the bond condition for each individual case, to avoid any serious interfacial failures, under the premise of achieving a satisfying reinforcement effectiveness.
- From the preventing pipe leakage point of view, composite reinforcement is more efficient on surface cracks with smaller aspect ratio. Reinforcement is also more effective on pipes with smaller external diameter and thinner wall thickness. Using high elastic modulus CFRP and more numbers of CFRP laminates are recommended for larger dimensional pipes to achieve a satisfying consequence.

CRediT authorship contribution statement

Zongchen Li: Conceptualization, Methodology, Validation, Formal analysis, Data curation, Writing – original draft, Writing – review & editing, Visualization. **Xiaoli Jiang:** Conceptualization, Supervision. **Hans Hopman:** Supervision, Funding acquisition.

Declaration of Competing Interest

The authors declare that they have no known competing financial interests or personal relationships that could have appeared to influence the work reported in this paper.

Acknowledgement

The authors appreciate the Department of Maritime and Transport Technology, Delft University of Technology, the Netherlands for sponsoring this research. The first author would like to acknowledge the China Scholarship Council, P. R. China [grant number 201606950024], for supporting his research.

Appendix A. . Comparison of the SIF results evaluated by ABAQUS and ANSYS [2]

Table A1 and A2.

Table A1
SIF along the surface crack front (eccentric angle from 0 to 90°) of a small crack and a large crack evaluated by ABAQUS.

Eccentric angle (°)	Small crack SIF (MPa•mm$^{1/2}$)	Large crack SIF (MPa•mm$^{1/2}$)
0	935.72	1475.35
2.95	965.16	1497.06
5.90	953.78	1479.65
8.85	932.34	1442.64
11.80	918.90	1391.72
14.75	906.80	1348.24
17.70	903.41	1316.53
20.66	896.95	1298.49
23.61	889.67	1280.74
26.56	883.00	1264.38
29.51	878.69	1252.94
32.46	874.38	1237.84
35.41	871.92	1227.93
38.36	869.36	1216.45
41.31	867.92	1204.92
44.26	866.48	1195.38
47.21	865.77	1188.09
50.16	865.05	1183.47
53.11	864.74	1178.83
56.07	864.43	1170.92
59.02	864.43	1163.25
61.97	864.33	1154.09
64.92	864.43	1145.87
67.87	864.43	1138.34
70.82	864.64	1134.65
73.77	864.74	1131.98
76.72	864.43	1129.45
79.67	855.82	1125.6
82.62	859.10	1122.36
85.57	862.38	1119.34
88.52	864.23	1120.54

Table A2
SIF along the surface crack front (eccentric angle from 0 to 90°) of a small crack and a large crack evaluated by ANSYS.

Eccentric angle (°)	Small crack SIF (MPa•mm$^{1/2}$)	Large crack SIF (MPa•mm$^{1/2}$)
0	946.53	1480.0
6	974.95	1508.0
12	938.05	1422.6
18	897.11	1338.0
24	892.69	1312.3
30	878.3	1271.1
36	877.22	1250.2
42	869.93	1219.1
48	871.29	1204.5
54	866.73	1181.0
60	868.24	1170.5
66	864.57	1154.7
72	867.15	1146.4
78	864.96	1133.2
84	867.43	1127.9
90	864.74	1117.7

Appendix B. . SIF results of PE-1 and PE-1-R simulated during the crack propagation process

Table B1.

Table B1
SIF results of PE-1 and PE-1-R models.

Specimen	PE-1				PE-1-R			
No.	*a*	*c*	Δ *Ka*	Δ *Kc*	*a*	*c*	Δ *Ka*	Δ *Kc*
0	4.29	5.795	639.09	710.1	5.98	7.12	635.301	637.722
1	4.784884	6.317235	684.3123	760.347	6.332774	7.467657	648.603	649.962
2	5.372857	6.993709	737.3025	819.225	6.713376	7.841253	663.129	665.073
3	6.092555	7.890833	803.5605	892.845	7.126153	8.248804	678.465	698.724
4	7.007028	9.133369	889.218	988.02	7.574998	8.740072	698.211	735.552
5	8.241303	10.95647	1011.933	1124.37	8.073592	9.336768	719.784	748.323
6	10.0003	13.93027	1197.423	1330.47	8.630994	9.973635	742.887	762.498
7	12.30006	18.47165	/	/	9.256802	10.65738	766.314	809.289
8	/	/	/	/	9.958009	11.51401	796.347	837.378
9	/	/	/	/	10.76528	12.48873	841.401	883.503
10	/	/	/	/	11.7529	13.68277	/	/

References

[1] Z. Li, X. Jiang, H. Hopman, Surface Crack Growth in Offshore Metallic Pipes under Cyclic Loads: A Literature Review, J. Marine Sci. Eng. 8 (5) (2020) 339.
[2] Z. Li, X. Jiang, H. Hopman, L. Zhu, Z. Liu, An investigation on the circumferential surface crack growth in steel pipes subjected to fatigue bending, Theor. Appl. Fract. Mech. 105 (2020), 102403.
[3] DNV, DNV-RP-F108: Assessment of flaws in pipeline and riser girth welds. 2017.
[4] N. Saeed, H. Ronagh, A. Virk, Composite repair of pipelines, considering the effect of live pressure-analytical and numerical models with respect to ISO/TS 24817 and ASME PCC-2, Compos. B Eng. 58 (2014) 605–610.
[5] T. Tafsirojjaman, S. Fawzia, D. Thambiratnam, X.-L. Zhao, Behaviour of CFRP strengthened CHS members under monotonic and cyclic loading, Compos. Struct. 220 (2019) 592–601.
[6] Z. Li, X. Jiang, H. Hopman, L. Zhu, Z. Liu, External surface cracked offshore steel pipes reinforced with composite repair system subjected to cyclic bending: An experimental investigation, Theor. Appl. Fract. Mech. 109 (2020), 102703.
[7] R. Branco, F.V. Antunes, J.D. Costa, A review on 3D-FE adaptive remeshing techniques for crack growth modelling, Eng. Fract. Mech. 141 (2015) 170–195, https://doi.org/10.1016/j.engfracmech.2015.05.023.
[8] M.A. Ghaffari, H. Hosseini-Toudeshky, Fatigue crack propagation analysis of repaired pipes with composite patch under cyclic pressure, J. Pressure Vessel Technol. 135 (3) (2013), 031402.
[9] Z. Li, X. Jiang, H. Hopman, Numerical analysis on the SIF of internal surface cracks in steel pipes reinforced with CRS subjected to bending, Ships Offshore Struct. (2019) 1, https://doi.org/10.1080/17445302.2019.1702769.
[10] Z. Li, X. Jiang, H. Hopman, L. Zhu, Z. Liu, Numerical investigation on the surface crack growth in FRP-reinforced steel plates subjected to tension, Theor. Appl. Fract. Mech. 108 (2020), 102659.
[11] H. Zarrinzadeh, M.Z. Kabir, A. Deylami, Crack growth and debonding analysis of an aluminum pipe repaired by composite patch under fatigue loading, Thin-Walled Struct. 112 (2017) 140–148.
[12] B. Zheng, M. Dawood, Fatigue crack growth analysis of steel elements reinforced with shape memory alloy (SMA)/fiber reinforced polymer (FRP) composite patches, Compos. Struct. 164 (2017) 158–169.
[13] T. Belytschko, T. Black, Elastic crack growth in finite elements with minimal remeshing, Int. J. Numer. Meth. Eng. 45 (5) (1999) 601–620.
[14] J. Fish, The s-version of the finite element method, Comput. Struct. 43 (3) (1992) 539–547.
[15] T.N. Nguyen, C.H. Thai, A.-T. Luu, H. Nguyen-Xuan, J. Lee, NURBS-based postbuckling analysis of functionally graded carbon nanotube-reinforced composite shells, Comput. Methods Appl. Mech. Eng. 347 (2019) 983–1003.
[16] H. Nguyen-Xuan, G.R. Liu, S. Bordas, S. Natarajan, T. Rabczuk, An adaptive singular ES-FEM for mechanics problems with singular field of arbitrary order, Comput. Methods Appl. Mech. Eng. 253 (2013) 252–273.
[17] M. Bocciarelli, P. Colombi, T. D'Antino, G. Fava, Intermediate crack induced debonding in steel beams reinforced with CFRP plates under fatigue loading, Eng. Struct. 171 (2018) 883–893.
[18] B. Zheng, M. Dawood, Debonding of carbon fiber–reinforced polymer patches from cracked steel elements under fatigue loading, J. Compos. Constr. 20 (6) (2016) 04016038.
[19] Z. Li, X. Jiang, H. Hopman, L. Zhu, Z. Liu, W. Tang, Experimental investigation on FRP-reinforced surface cracked steel plates subjected to cyclic tension, Mech. Adv. Mater. Struct. (2020) 1–15.
[20] *API SPEC 5L:Specification for Line Pipe*, API, WASHINGTON, D.C., 2018.
[21] Faserverbundwerkstoffe. "Technical data: Epoxy resin L 20." https://www.swiss-composite.ch/pdf/t-Epoxydharz-L20-e.pdf (accessed).
[22] S. Xia, J. Teng, Behaviour of FRP-to-steel bonded joints, in: presented at the Proceedings of the International Symposium on Bond Behaviour of FRP in Structures, Hong Kong, 7–9 December 2005, 2005, 419–426.
[23] Abaqus. "Test Configurations for Abaqus 2021 Products." Dessault System. https://www.3ds.com/support/hardware-and-software/simulia-system-information/abaqus-2021/ (accessed).
[24] ANSYS. "Ansys 2021 R2 Release Highlights." https://www.ansys.com/products/release-highlights (accessed).
[25] P. Paris, F. Erdogan, A critical analysis of crack propagation laws, J. Basic Eng. 85 (4) (1963) 528–533.